Crystallization in Polyamide 6/Polysulfone Blends: Effect of Polysulfone Particle Size

Piyada Charoensirisomboon, Hiromu Saito, and Takashi Inoue*

Department of Organic and Polymeric Materials, Tokyo Institute of Technology, Ookayama Meguro-ku Tokyo 152, Japan

Martin Weber and Eckhard Koch

BASF, Polymer Research Laboratory, D-67056, Ludwigshafen, Germany

Received January 14, 1998; Revised Manuscript Received May 29, 1998

ABSTRACT: By reactive blending of polyamide 6 (PA) with polysulfone (PSU) using a gram-scale mixer (Mini-Max Molder), we prepared a series of PA/PSU (80/20 wt.ratio) with various diameters of PSU particles: 90 nm by using phthalic anhydride-terminated PSU (PSU−PhAH), 0.2 μm by carboxylic acid-grafted PSU (PSU−COOH), and 1.0 μm by nonreactive PSU (nf-PSU). Isothermal crystallization was carried out at 200 °C. Light scattering studies showed that spherulites in the blends can grow to more than 10 μm in diameter, as in the case of neat PA. It suggests that crystal growth in the radial direction can be achieved by circumventing the PSU obstacles; i.e., it does not matter how big or small they are in the range of 90 nm to 1 μm. The smaller the PSU particles, the slower was the overall rate of crystallization. The slower rate may be caused by the higher population of brush PA chains attached to PSU particles as block or graft chains, since the brushes may be hard to organize into crystal lamellae, compared with free chains. The blends showed rather broad wide-angle X-ray diffraction profiles. The smaller the PSU particles, the broader was the profile. The scattering from the particles themselves should appear only at extremely low angles (<0.1°) and hardly affects the wide-angle X-ray profiles so that the results may imply that the presence of smaller PSU particles renders the less perfection of the PA crystal. This may be caused also by the higher population of brush chains. Note that the brush chains are formed only in the reactive systems and the population may be higher in the smaller particle systems. Even for the blend with smallest particle size, a small-angle X-ray scattering peak appeared at a magnitude of scattering vector of ~0.8 nm^{-1}, suggesting the evolution of interlamellar spacing of 8.7 nm. However, the scattering profile was much broader than that of neat PA. It implies a less ordered lamellar stacking in the blend.

Introduction

Blending of dissimilar polymers to produce high-performance materials is attracting great attention. Immiscible polymers are mostly dealt with by reactive blending. The reactive blending involves in-situ reaction of functionalized components to form a block or graft copolymer at the interface between phases.[1−7] The copolymer formation is known to be effective for morphology control. For polymer blends in which one of the components is crystallizable, the presence of the other components may affect the crystallization process. Both the crystallization kinetics and the final crystal morphology may be very different from that of the neat crystallizable component. As reviewed by Martuscelli,[8] such differences have been found in various blends. In the previous article,[9] we demonstrated that by reactive blending of polyamide 6 (PA) with polysulfone (PSU), a series of 80/20 blends with various diameters of PSU particles can be prepared: 50 nm by using phthalic anhydride-terminated PSU, 0.27 μm by carboxylic acid-grafted PSU, and 1.0 μm by nonreactive PSU. The specimens provide a nice opportunity to study the effect of impurity (PSU) particle sizes on the crystallization of matrix polymer (PA), which has not been studied so far.

In this paper, we carried out isothermal crystallization of neat PA and PA/PSU blends at a crystallization temperature higher than the glass transition temperatures of both PA and PSU. Development of PA crystallite is analyzed by a time-resolved light scattering photometer equipped with a highly sensitive charge-coupled device (CCD) camera. Crystalline morphologies at both lamella and unit cell levels are also studied by small-angle X-ray scattering and wide-angle X-ray diffraction.

Experimental Section

The PA used was a commercial polyamide 6 (Ultramid B, BASF). PSU without a functional group (nf-PSU) was synthesized by reacting dichlorodiphenyl sulfone with Bisphenol A in the presence of K_2CO_3 in dry *N*-methyl-2-pyrrolidone

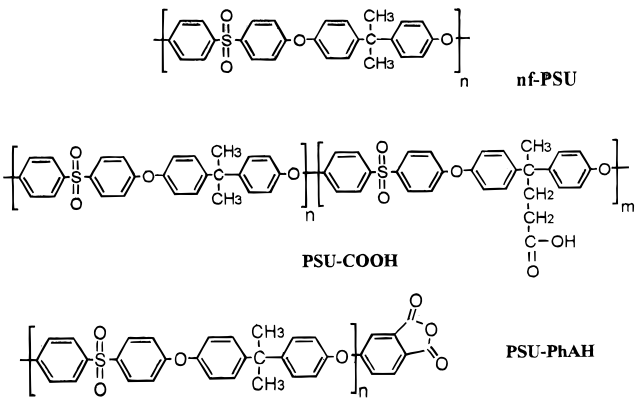

* To whom correspondence should be addressed.

S0024-9297(98)00048-5 CCC: $15.00
Published on Web 07/10/1998

Table 1. Characteristics of Polymers

code	M_n[a]	M_w[a]	functionality[b]	T_g[c]
PA	13000	25 000		
nf-PSU	5700	28 800		183
PSU−COOH	5300	23 700	84	178
PSU−PhAH	5310	20 661	85	157

[a] GPC measurement. [b] Content of functional group, μmol/g. [c] DSC measurement, °C.

(NMP). The amount of chlorine end groups was detected by elemental analysis to be 98 wt %. PSU−COOH was prepared by reacting dichlorodiphenyl sulfone, Bisphenol A, and a small amount of diphenolic acid (DPA) in the presence of K_2CO_3 in dry NMP. The amount of incorporated DPA units was estimated by ^{1}H NMR spectroscopy (in $CDCL_3/CF_3COOD$ 1/1). PSU−PhAH was prepared by adding 4-fluorophthalic anhydride to the as-polymerized solution of nf-PSU. The amount of anhydride end groups was determined by FT-IR. Details of preparation procedures are given elsewhere.[9−12] The characteristics of polymers are summarized in Table 1.

PA pellets were dried under vacuum (10^{-4} mmHg) at 80 °C for 12 h before mixing to remove water completely. PA and PSU were melt-mixed in a miniature mixer of one gram-scale, Mini-Max Molder (CS-183 MNX, Custom Scientific Instruments, Inc.), at 260 °C for 8 min with the rotor speed set at 100 rpm. The weight ratio of PA/PSU was fixed at 80/20. The melt was extruded, chopped into pellets, and again dried under vacuum at room temperature for 24 h.

The two-phase structure of blends was examined by transmission electron microscopy (TEM). The specimen was cryomicrotomed at −65 °C by an ultramicrotome (Reichert Ultracut-Nissei). The ultrathin section of ca. 60 nm thickness was mounted on a 200 mesh copper grid and exposed to the vapor of ruthenium tetroxide (RuO_4) above a 0.5 wt % aqueous solution of RuO_4 for 10 min. RuO_4 preferentially stains the PSU phase to provide a nice contrast under TEM. The two-phase morphology was observed by transmission electron microscope, JEM-100CX (JEOL), at an accelerating voltage of 100 keV. The TEM picture was digitized using a scanner (EPSON GT8500). The area of an individual particle a_i was directly determined using a software (PIAS-VII-Personal Image Analysis System). The diameter of the dispersed particles D_i was calculated by $D_i = 2(a_i/\pi)^{1/2}$, assuming the shape of particle to be circular. Then the average diameter was obtained by

$$D_{TEM} = \sum_{i=1}^{N} D_i^3 / \sum_{i=1}^{N} D_i^2$$

where N was 200−500 in a TEM picture. The average by this equation may be appropriate for the comparison with that by light scattering because the particle size by light scattering is based on the interfacial area,[7] which corresponds to the ratio of volume-average diameter (numerator) and surface-average diameter (denominator).

A thin film specimen (ca. 15 μm thick) was prepared by pressing the small pieces of pellet between two cover glasses at 260 °C. After the specimen was held at 260 °C (above the melting point of PA) for 2 min, it was rapidly transferred to a light scattering hot stage set at a crystallization temperature (T_c = 200 °C). Isothermal crystallization at T_c was investigated by time-resolved light scattering. The light scattering apparatus is shown schematically in Figure 1. A polarized He−Ne laser of 632.8 nm wavelength was applied vertically to the film specimen. The scattered light was passed through an analyzer. We employed two optical geometries: one was the H_v geometry in which the optical axis of the analyzer was set perpendicularly to that of the polarizer and the other was the V_v geometry with a parallel set of the two axes. The angular distribution of light scattering intensity was detected by the highly sensitive CCD camera with 576 × 382 pixels (Princeton Instruments, Inc.).[13] To estimate the PSU particle size in the as-mixed blend, the V_v scattering profile just after

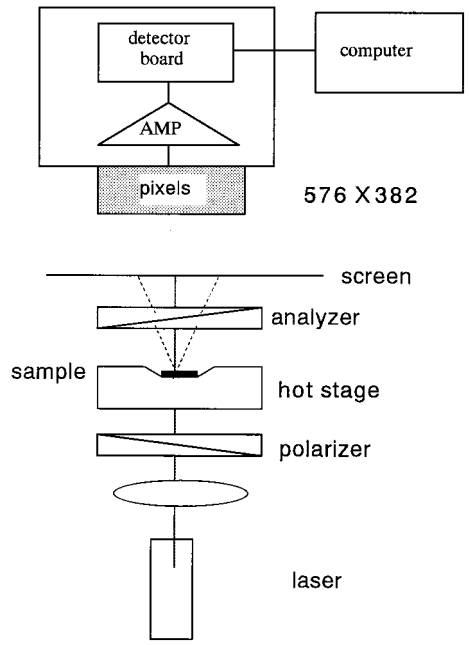

Figure 1. Light scattering apparatus.

the remelt at 260 °C was also measured and the result was analyzed by using the Debye−Bueche plot.[4,7]

Optical microscopic observation during the isothermal crystallization was also carried out under a polarized optical microscope (Olympus BH-2).

A thick specimen (ca. 0.5 mm thick) was also prepared by pressing between two polyimide sheets at 260 °C for 2 min, and it was rapidly transferred into a hot stage set at the crystallization temperature. After annealing for a given time, the specimen was quickly quenched into an ice water bath to freeze the structure developed during the isothermal annealing. The wide-angle X-ray diffraction (WAXD) profile of the annealed specimen was observed by a Rigaku Denki RU-200 X-ray diffraction apparatus. The radiation from the Cu anode was reflected from a graphite monochromator to obtain monochromatic Cu Kα radiation with a wavelength of 0.1542 nm. The generator was operated at 40 kV and 180 mA. The WAXD experiments were performed at room temperature.

The X-ray source used for small-angle X-ray scattering (SAXS) was the same as for WAXD. The scattering intensity, I, was corrected for background scattering after a smoothing procedure. The scattering intensity by thermal fluctuations was subtracted from the SAXS profile $I(q)$ by plotting $I(q)q^3$ versus q^3 for slit collimation at large q range, where q is the magnitude of the scattering vector defined by $(4\pi/\lambda) \sin \theta^{-1}$, λ and θ being the wavelength and the scattering angle, respectively. From the corrected profile, the Bragg spacing was obtained as the interlamellar distance $L = 2\pi/q_m$, where q_m is the peak maximum in the Lorentz-corrected plot, Iq^2 versus q.

Thermal analysis was carried out by a differential scanning calorimeter, Seiko EXSTAR6000. The specimen packed in an aluminum pan was heated to 260 °C and kept at this temperature for 5 min under a nitrogen atmosphere to erase the previous thermal history. Then the sample was rapidly cooled to the T_c and was isothermally crystallized for 1 h. Then, a heating scan was performed at a heating rate of 20 °C min^{-1}. The melting temperature and the enthalpy of fusion were obtained from the maximum and the area of the endothermic peak, respectively. The crystallinity X_c was calculated by $X_c = \Delta H^*/\Delta H^\circ_{PA6}$, where ΔH^* is the enthalpy of fusion per gram of PA or in the blend and ΔH^0_{PA6} is the enthalpy of fusion per gram of 100% crystalline PA (=230 J/g).[14]

Results and Discussion

The TEM pictures of PA/PSU blends are shown in Figure 2. The darker phase is PSU stained by RuO_4.

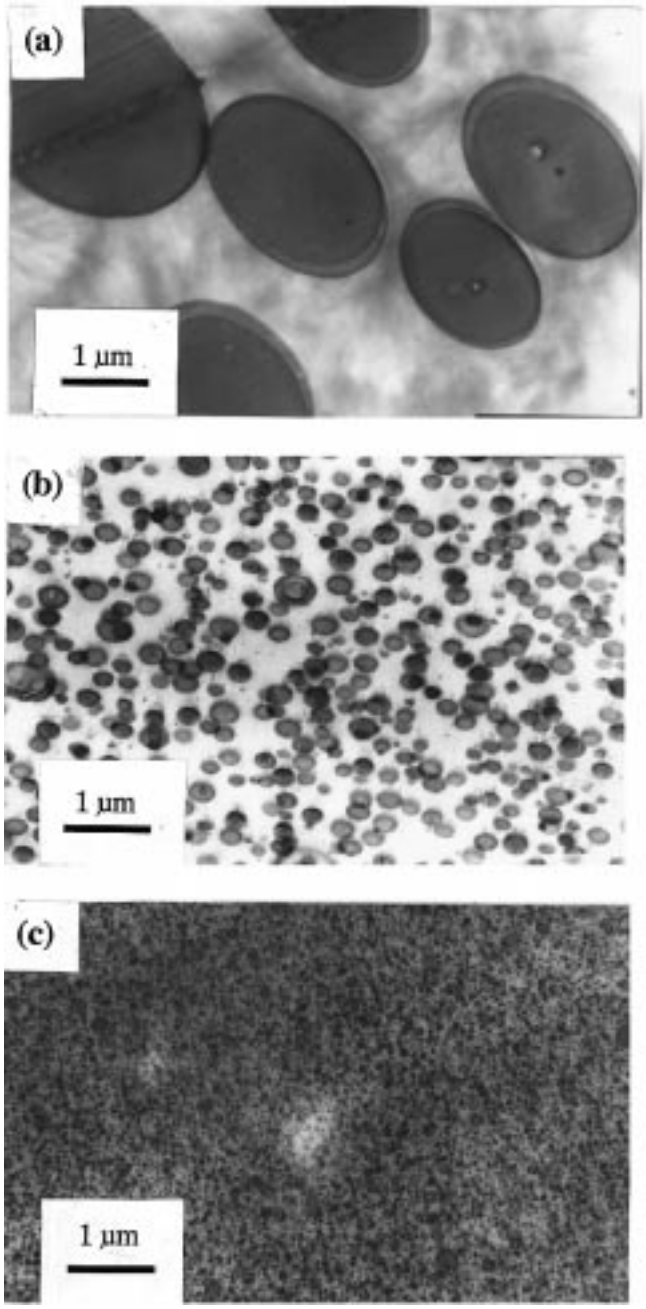

Figure 2. TEM micrographs of melt-mixed 80/20 PA/PSU blends at 260 °C for 8 min: (a) PA/nf-PSU; (b) PA/PSU-COOH; (c) PA/PSU-PhAH.

Compared with nonreactive system (Figure 2a), the reactive systems yield much smaller particles (Figure 2b, c). The results are expected, since the reactive systems may generate the PSU−PA graft or block copolymer, which would play a role of emulsifier to reduce the interfacial tension and prevent particle coalescence. The calculated average particle diameters are listed in Table 2, with a nice agreement with those by light scattering. Thus, we prepared a series of blend specimens having various particle diameters ranging from 90 nm to 1 μm. Note that some gray textures are seen in the matrix of Figure 2a, reflecting probably a crystalline morphology of PA. They are obvious only in the nonreactive blend. It may suggest that appreciable crystallization took place during extrusion (slow cooling) in the nonreactive system but the crystallization rate in the reactive systems may be much slower. This point will be discussed later.

Table 2. PSU Particle Diameters in Blends Mixed at 260 °C for 8 min

code	D^*_{scatt}/μm	D_{TEM}/μm
PA/nf-PSU	1.02	1.20
PA/PSU−COOH	0.28	0.27
PA/PSU−PhAH	0.07	0.097

[a] By the Debye−Bueche plot of the V_v scattering profile[4,7] at 260 °C ($> T_m$).

Figure 3 shows the polarized optical micrographs of the isothermally crystallized thin films of neat PA and the blends. One sees the same spherulitic nature in all specimens. However, both Maltese crosses and zero-birefringence extinction rings are not clear, suggesting the formation of disordered spherulites.

The spherulitic nature is revealed by the H_v light scattering patterns, as typically shown in Figure 4. The four-leaf-clover pattern in the H_v mode is characteristic of the spherulite, and it is ascribed to the ordering of the optical axis in both tangential and radial directions within the spherulite. From one-dimensional H_v scattering profiles at azimuthal angle 45° in the scattering patterns, one can discuss the details of spherulite morphology as follows.

As expected from the four-leaf-clover patterns, the one-dimensional scattering profiles shown in Figure 5 obviously have scattering maxima. From the peak angle θ_m, the average radius of spherulite R_{H_v} can be estimated by

$$4.1 = 4\pi(R_{H_v}/\lambda') \sin(\theta_m/2) \quad (1)$$

where λ' is the wavelength of light in medium.[15] The estimated radii are shown in Figure 6 as a function of crystallization time. Unfortunately, the peaks were not clear at the early stages of crystallization so that time variations are shown just for the late stages. Anyhow, the results in Figures 5 and 6 clearly show that the spherulites can grow up to more than 10 μm in diameter even in blends. It suggests that crystals can grow by circumventing the obstacles of PSU particles, no matter how small or big they are in a range of 10 nm to 1 μm. The smaller particle system yields the smaller spherulite; however, the difference is not so big.

By the one-dimensional H_v scattering profile, one can also discuss the ordering in the spherulite. To discuss the ordering process within the spherulite, it is convenient to employ an order parameter P_r. According to Yoon and Stein,[16] the relative intensity of scattered light at small angles ($\theta < \theta_m$) is enhanced by the disordering of the orientation fluctuation in the tangential direction, while at wide angles ($\theta > \theta_m$), it is enhanced by the disordering in the radial direction. P_r should be given by using the reduced scattering angle w

$$w = (2\pi/\lambda)R_{H_v} \sin\theta \quad (2)$$

Then P_r is defined by

$$P_r = I_{H_v}(w = 4)/I_{H_v}(w = 8) \quad (3)$$

The calculated results of R_{H_v} and P_r for crystallized samples at 200 °C for 30 min are summarized in Table 3. Compared with neat PA, the PA/nf-PSU blend has a lower ordering. The presence of PSU particles of 1

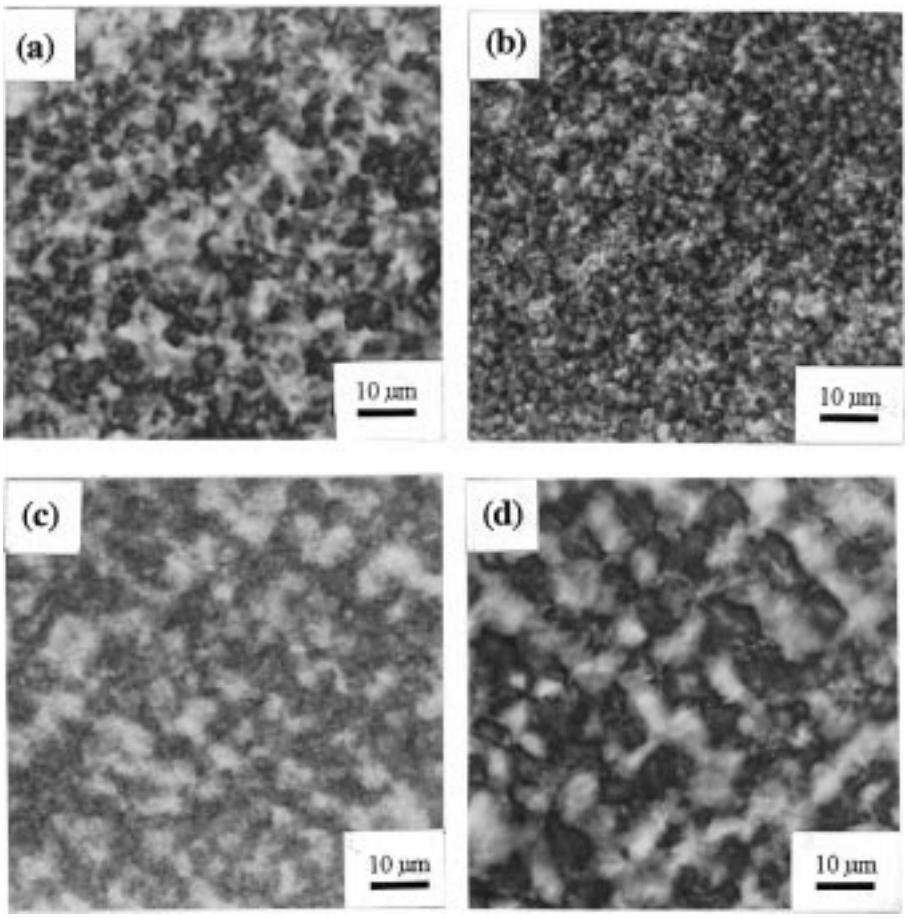

Figure 3. Polarized optical micrographs after isothermal crystallization at 200 °C for 60 min: (a) neat PA; (b) PA/nf-PSU; (c) PA/PSU-COOH; (d) PA/PSU-PhAH.

Table 3. Spherulite Radii and Order Parameters; Crystallized at T_c = 200 °C, 30 min

code	R_{H_v}/μm	P_r
neat PA	21.03	1.84
PA/nf-PSU	16.31	1.08
PA/PSU−COOH	16.06	1.20
PA/PSU−PhAH	14.88	1.97

μm diameter could cause a serious circumvention for the radial growth of the spherulite to render the lower ordering. It is interesting that the reactive (PA/PSU−COOH and PA/PSU−PhAH) systems with smaller obstacles have higher orderings than the nonreactive blend. The higher ordering may be caused by a kinetic reason; i.e., the slower crystal growth is expected to yield the higher ordering. The smaller difference in spherulite size (R_{H_v}) may be caused mostly by the difference in nucleation density.

For kinetic discussion, one can employ the integrated scattering intensity, the invariant Q:[17]

$$Q = \int_0^\infty I(q)\, q^2\, \mathrm{d}q \tag{4}$$

The invariant in the H_v mode, Q_{H_v}, is described by the mean-square optical anisotropy $\langle\delta^2\rangle$

$$Q_{H_v} \propto \langle\delta^2\rangle = \phi_s(\alpha_r - \alpha_t)^2 \tag{5}$$

where ϕ_s is the volume fraction of spherulites and α_r and α_t are the radial and tangential polarizabilities of the spherulites, respectively. The invariant in the V_v mode, Q_{V_v}, is ascribed to both $\langle\delta^2\rangle$ and the mean-square density fluctuation $\langle\eta^2\rangle$. The $\langle\eta^2\rangle$ is given by

$$\langle\eta^2\rangle = \phi_s(1 - \phi_s)(\alpha_s - \alpha_0)^2 \tag{6}$$

where α_s is the average polarizability of the spherulite and α_o is the polarizability of the melt.

The time variations of the invariant Q_{H_v} and Q_{V_v} of neat PA and a reactive blend at T_c = 200 °C are shown in Figure 7. As expected from eq 6, Q_{V_v} attains a maximum when ϕ_s reaches 0.5, since the anisotropy contribution $\langle\delta^2\rangle$ is small enought to be neglected. The time to attain 50% volume filling may be assumed to be a rate constant for spherulite growth. It is ca. 70 s for neat PA (Figure 7a) and 160 s for the PA/PSU−PhAH blend (Figure 7b). The time variations of invariants for nf-PSU and PSU−COOH systems are not shown in Figure 7. But the peak times were 75 and 90 s, respectively. The results show that the smaller the PSU particle size, the slower is the spherulite growth.

On the other hand, Q_{H_v} gradually increases with time and then levels off. The values of Q_{H_v} at early stages were divided by the leveled off value. To discuss the kinetics, the normalized Q_{H_v} is plotted as a function of time in Figure 8. The initial slope of normalized Q_{H_v}, $\mathrm{d}Q_{H_v}/\mathrm{d}t$, is supposed to be a rate of crystallization. It shows that the overall crystallization rate of PA is suppressed in reactive blends. The smaller the PSU particles, the slower is the overall rate of crystallization. The slower rate may be caused by the higher population of brush PA chains attached to PSU particles as block or graft chains, since the brushes may be hard to

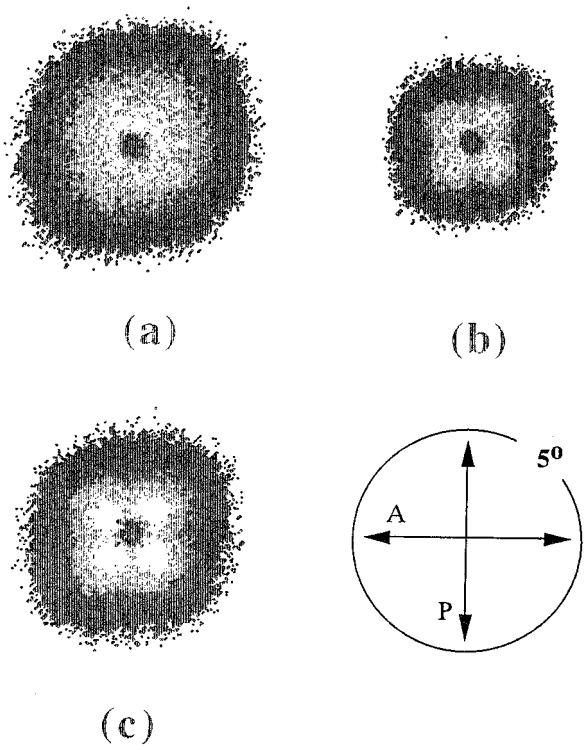

Figure 4. H_v light scattering patterns; after crystallization at $T_c = 200$ °C for 750 s: (a) neat PA; (b) PA/PSU-COOH; (c) PA/PSU-PhAH. A = analyzer (horizontal), P = polarizer (vertical), 5° = scattering angle.

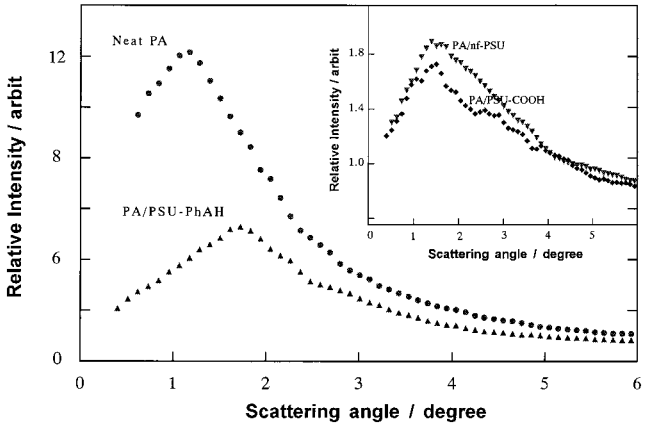

Figure 5. H_v light scattering profiles at azimuthal angle $\mu = 45°$: (●) neat PA; (▲) PA/PSU-PhAH; (◆) PA/PSU-COOH, (▼) PA/nf-PSU.

organize into crystal lamellae, compared with free chains. In addition, the apparent induction time, t_o, in the smaller particle system is longer. It may be caused by the same scenario.

Figure 9 shows Lorentz-corrected SAXS profiles of the annealed sample at $T_c = 200$ °C for 60 min. A peak around the scattering vector $q \cong 0.6-0.8$ nm^{-1} corresponds to the long spacing, L (or interlamellar distance), of ca. 10 nm. The results imply that PSU particles do not reside in the interlamellar region. The broader scattering profiles of reactive blends suggest less ordering in the lamellar arrangement than in neat PA. The less ordering could be caused by the stronger spatial restriction for lamellar stacking and/or the higher population of brush chains in the blends with smaller PSU particles. Note that the smaller particle system has the lower ordering in lamellar stacking but the

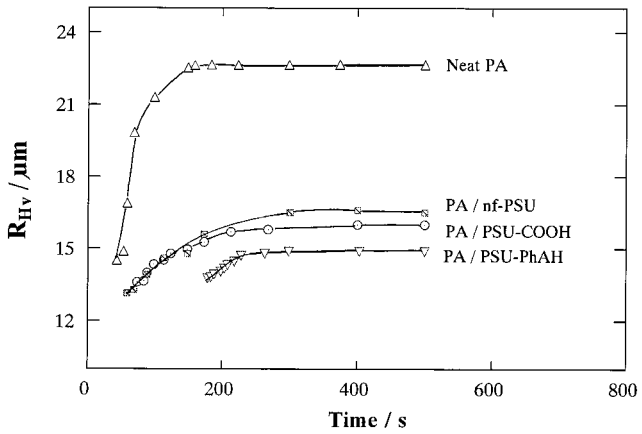

Figure 6. Time variation of the spherulite radii of neat PA and blends at 200 °C: (△) neat PA; (□) PA/nf-PSU; (○) PA/PSU-COOH; (▽) PA/PSU-PhAH.

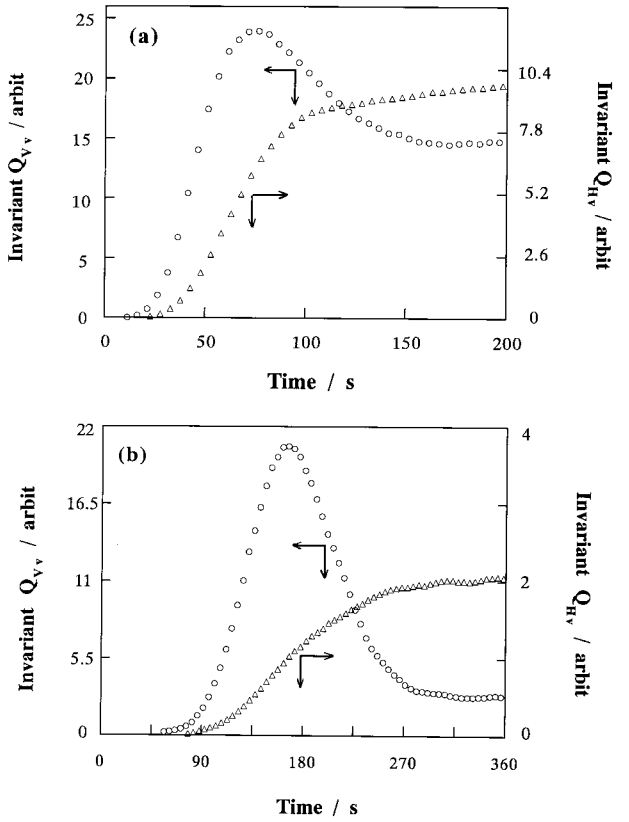

Figure 7. Time variation of the invariants under V_v and H_v modes at $T_c = 200$ °C: (a) neat PA; (b) PA/PSU-PhAH.

higher ordering in the orientation fluctuation of stacked lamellae in the spherulite (see Table 3)

The results of thermal analysis by DSC are summarized in Table 4. The reactive blends with smaller PSU particles (PSU−COOH and PSU−PhAH systems) have slightly lower melting points and slightly smaller crystallinities than those of neat PA and the nonreactive system. Combining the DSC and SAXS results, the lamellar thickness L_c can be estimated by $L_c = X_c L$, X_c being the crystallinity. The calculated L_c values are also listed in Table 4.

It is well-known that PA has a polymorphy, and different crystalline forms may develop depending on the thermal treatment, the state of orientation and deformation, and the interaction with other components. Then, it is also interesting to know whether the PSU

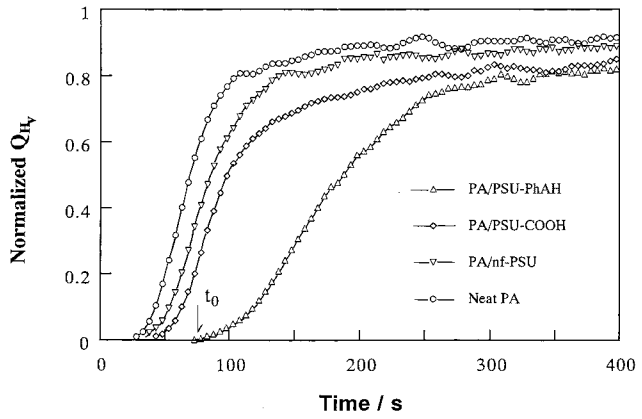

Figure 8. Time variation of normalized Q_{H_v} during crystallization at T_c = 200 °C.

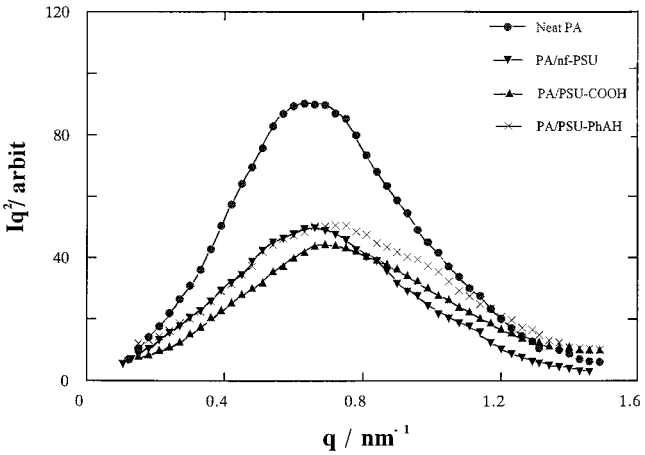

Figure 9. Lorentz-corrected SAXS profiles; after the crystallization at T_c = 200 °C for 1 h.

Table 4. Results by DSC and SAXS

code	T_m/°C	X_c/wt %	L/nm	L_c/nm
neat PA	218.6	32.8	9.7	3.1
PA/nf-PSU	218.5	26.7 (32.3)[a]	9.7	2.5
PA/PSU−COOH	217.4	23.9 (30.0)[a]	9.0	2.1
PA/PSU−PhAH	217.5	25.0 (30.6)[a]	8.7	2.2

[a] X_c: per gram of PA.

particles affect polymorphy or not. WAXD profiles in Figure 10 show that there is no essential difference in diffraction positions between the blends and neat PA. Two distinct diffraction peaks at diffraction angles 2θ = 20.08° and 23.8° can be assigned to (200) and (202) + (002) reflections, respectively. The results imply the monoclinic α form[18] in both PA and the blends. It is interesting to note a difference in the relative intensity of the (200) reflection and (202) + (002) reflections. Neat PA show a (202) + (002) peak stronger than the (200) peak, while the PSU−PhAH system has almost same intensity for the two peaks. The results imply that the crystal lattice in the direction perpendicular to the (200) plane is less ordered in the PSU−PhAH system. The reason is not obvious at present.

Conclusion

The effect of PSU particles on the isothermal crystallization of the PA matrix was studied by light scattering, SAXS, WAXD, and DSC. The spherulite with a radius of more than 10 μm develops despite the presence of the PSU obstacles. However, the rate of crystallization

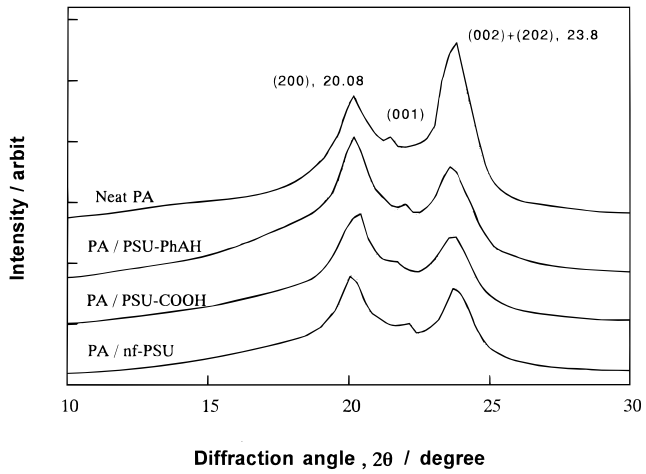

Figure 10. Wide-angle X-ray diffraction profiles; after the crystallization at T_c = 200 °C for 1 h.

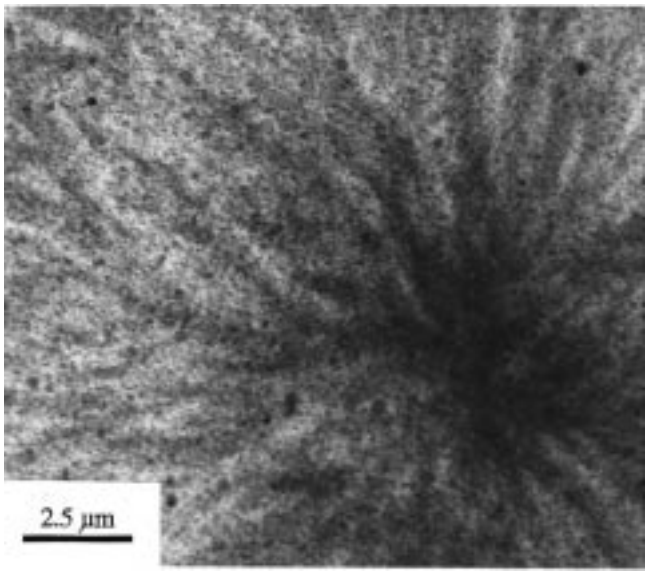

Figure 11. TEM micrograph of the PA/PSU-PhAH blend crystallized at 200 °C for 1 h. Double staining by RuO_4 and phosphotungstic acid was successfully applied to visualize the spherulitic nature.

was slowed and the onset was delayed by the presence of PSU particles. The smaller the particles, the slower was the rate. The smaller PSU particle yielded the higher ordering in the spherulite structure and lower ordering in the lamellar stacking and crystal lattice. The slower crystallization rate and the lower ordering may be caused by the higher population of brush PA chains attached to PSU particles as block or graft chains.

Acknowledgment. The authors are grateful to the German Government, BMBF, for providing them a research fund (project 03N30283). We express our appreciation to T. Chiba and Dr. S. Asai, TIT, for helping with TEM and SAXS experiments, respectively.

Appendix

The scattering studies suggest that the PSU particles are not segregated out of the spherulite but reside in the spherulite. To confirm it, we tried to visualize the structure under TEM. We employed the double-staining method[7] for the TEM observation. The PA/PSU-PhAH blend crystallized at 200 °C for 1 h was micro-

tomed and first stained by a 10% aqueous solution of phosphotungstic acid at room temperature for 12 h. Then, the stained ultrathin section was further stained by RuO_4, as described in the Experimental Section. As shown in Figure 11, the spherulitic nature was revealed by the double-staining technique. The PSU particles remain in the spherulite, as expected. One can see also that the center of the spherulite is darker, i.e., stained more deeply. It implies the lower crystallinity and/or lower ordering in the lamellar stacking at the center. This is consistent with the result in Figure 6: the H_v scattering peak was not detected at the early stage of crystallization.

References and Notes

(1) Baker, W. E.; Saleen, M. *Polym. Eng. Sci.* **1987**, *27*, 1634.
(2) Angola, J. C.; Fujita, Y.; Sakai, T.; Inoue, T. *J. Polym. Sci., Polym. Phys. Ed.* **1988**, *26*, 807.
(3) Oshinski, A. J.; Keskkula, H.; Paul, D. R. *Polymer* **1992**, *33*, 268.
(4) Okamoto, M.; Inoue, T. *Polym. Eng. Sci.* **1993**, *33*, 175.
(5) Gonzalez, M. A.; Keskkula, H.; Paul, D. R. *J. Polym. Sci., Polym. Phys. Ed.* **1995**, *33*, 1751.
(6) Scott, E. C.; Macosko, C. W. *Polymer* **1995**, *36*, 461.
(7) Li, H.; Chiba, T.; Higashida, N.; Yang, Y.; Inoue, T. *Polymer* **1997**, *38*, 3921.
(8) Martuscelli, E. *Polym. Eng. Sci.* **1984**, *24*, 563.
(9) Ibuki, J.; Charoensirisomboon, P.; Ougizawa, T.; Inoue, T.; Weber, M.; Koch, E. *Polymer*, in press.
(10) Esser, IC. H. M.; Parsons, I. A. *Polymer* **1993**, *34*, 1836.
(11) Koch, H.; Ritter, H. *Makromol. Chem. Phys.* **1994**, *195*, 1709.
(12) DE-A 41 10 460, BASF AG.
(13) Lee, C.; Saito, H.; Inoue, T. *Macromolecules* **1993**, *26*, 6566.
(14) Dole, M.; Wunderlich, B. B. *Macromol. Chem.* **1959**, *34*, 29.
(15) Rhodes, M. B.; Stein, R. S. *J. Polym. Sci.* **1960**, *45*, 521.
(16) Yoon, D. Y.; Stein, R. S. *J. Polym. Sci., Polym. Phys. Ed.* **1974**, *12*, 763.
(17) Koberstein, T.; Russell, T. P.; Stein, R. S. *J. Polym. Sci., Polym. Phys. Ed.* **1979**, *17*, 1719.
(18) Holms, D. R.; Bunn, C. W.; Smith, D. J. *J. Polym. Sci.* **1955**, *27*, 159.

MA980048L